PERGAMON

International Journal of Multiphase Flow 28 (2002) 1895–1910

International Journal of Multiphase Flow

www.elsevier.com/locate/ijmulflow

Visual measurements of droplet size in gas–liquid annular flow

L.B. Fore *, B.B. Ibrahim, S.G. Beus

Bettis Atomic Power Laboratory, Bechtel Bettis Inc., West Mifflin, PA 15122, USA

Received 8 August 2000; received in revised form 26 September 2002

Abstract

Drop size distributions have been measured for nitrogen–water annular flow in a 9.67 mm hydraulic diameter duct, at system pressures of 3.4 and 17 bar and a temperature of 38 °C. These new data extend the range of conditions represented by existing data in the literature, primarily through an increase in system pressure. Since most existing correlations were developed from data obtained at lower pressures, it should be expected that the higher-pressure data presented in this paper would not necessarily follow those correlations. For two volume median correlations tested, one does not predict the new data very well, while the other only predicts those data taken at the lower pressure of 3.4 atm. An existing maximum drop size correlation predicts the current data to a reasonable approximation. Similarly, a related correlation for the Sauter mean diameter can predict the new data, provided the coefficient in the equation is adjusted.

1. Introduction

Two-phase gas–liquid flow occurs in a variety of industrial situations including boilers, gas–liquid contacting systems and natural gas production wells. Annular flow, one of the most common regimes in two-phase flow, is characterized by a thin liquid film distributed along the perimeter of a conduit with a core of gas flowing in the center of the conduit. One of the distinguishing features of annular flow is the entrainment and deposition process. For liquid flow rates above some critical value, droplets are torn from large disturbance waves on the liquid film, become entrained in the gas core and may eventually redeposit onto the film. In the core, droplet acceleration increases the overall pressure drop while the increased interfacial area represented by the droplets enhances heat and mass transport between the gas and liquid phases. For these reasons, characterization of the dispersed droplets is important for the modeling and prediction of momentum, heat and mass transfer in gas–liquid annular flow.

* Corresponding author.
E-mail address: forelb@bettis.gov (L.B. Fore).

0301-9322/02/$ - see front matter
PII: S0301-9322(02)00121-0

A number of experimental measurements of droplet size in annular flow have been performed over the years. Wicks and Dukler (1966) used two opposing needles with an adjustable gap to sense the presence of conducting water droplets larger than the gap spacing. The number of bridging events for each of a series of gap spacings within a fixed time period was then used to construct a drop size distribution. In a related technique, Tatterson et al. (1977) applied an electrical charge to a needle which then discharged proportionately with the mass of individual impacting droplets. Recently, Trabold et al. (1999) calculated mean drop sizes for Refrigerant-134a from measurements of void fraction, droplet velocity and droplet frequency obtained with a hot-film anemometry probe.

Cousins and Hewitt (1968) used axial-view photography through a special window mounted on the top of a tubular test section to capture images of droplets. Hay et al. (1996) illuminated the gas-droplet core with a laser sheet and took photographs through a window in the side of a tubular test section. In both of these studies, the drops were sized manually, with much larger sample sizes used in the more recent Hay et al. study. The commercial Malvern laser diffraction system has been used in annular flow work by Azzopardi et al. (1980, 1991) and in a number of related studies. The Semiat and Dukler (1981) laser-grating technique for both drop size and velocity was applied by Lopes and Dukler (1987) and Fore and Dukler (1995) to annular flow. The phase-Doppler technique, which also produces size and velocity measurements, has been used by Azzopardi and Teixeira (1994) in annular flow.

Azzopardi (1997) summarized most of the available annular flow drop size data, most of which were obtained for the air–water system at low pressures (<2 atm) and temperatures. Most available correlations (Tatterson et al., 1977; Kataoka et al., 1983; Ambrosini et al., 1991) were developed from particular data sets chosen from those listed above. Of these correlations, the one developed by Ambrosini et al. uses only data taken within the same group (Azzopardi et al., 1980, etc.). Instead of measuring individual drops, the laser diffraction method infers the size distribution from the interference pattern produced by passing a laser beam through the field of droplets. The droplets are usually implicitly assumed to follow a standard size or volume probability density function such as the Rosin–Rammler distribution, but recent results have shown a need for independence from any fixed type of distribution.

This paper presents new measurements of droplet size obtained for two-phase nitrogen–water annular flow at pressures of 3.4 and 17 atm, which substantially expands the pressure range above that represented by most available data. Video images of the gas-droplet core were obtained with an axial-view optical setup similar to that used by Cousins and Hewitt. The recorded images were then processed to obtain individual drop sizes, from which several weighted mean sizes were computed. The various mean drop sizes are tabulated and compared to existing correlations in order to assess the applicability of those correlations outside of the range of conditions over which they were developed.

2. Experimental

2.1. Flow loop and test section

Fig. 1 is a schematic of the test section and flow loop used to obtain the new drop size measurements presented in this paper. Both gas and liquid flow systems were operated as closed loops.

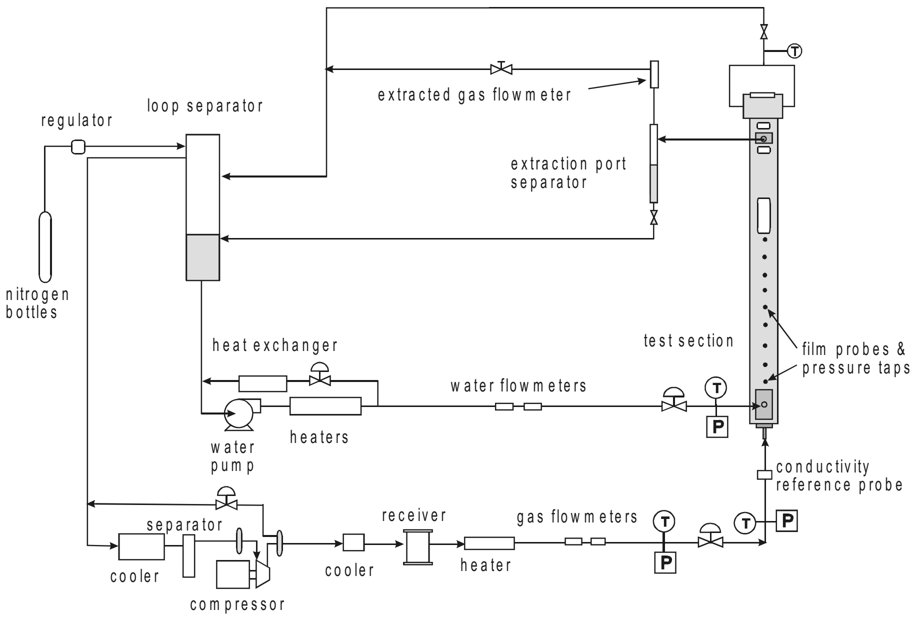

Fig. 1. Nitrogen–water flow loop and test section.

A large separator tank was used as a loop pressurizer and as the reservoir for gas and liquid. A centrifugal pump was used to circulate water from the separator, through a pair of Endress–Hauser Promass model 63F Coriolis flow meters installed in series, and to the liquid feed section of the test section. A reciprocating compressor was used to circulate nitrogen from the separator, through a pair of Rosemount model 8800 vortex flow meters installed in series, and to the test section gas inlet piping. The manufacturer-stated accuracies of the water and gas flow meters were $\pm 2\%$ and $\pm 1\%$, respectively. A gas heater was used to control the nitrogen temperature and several water heaters were used to control the water temperature. The system pressure was controlled by a pressure-regulated nitrogen supply attached to the top portion of the loop separator. Temperatures, measured with chromel–alumel thermocouples, are considered accurate within ± 2 °C and system gage pressures, measured with Rosemount Model 3051C pressure transmitters, were considered accurate within $\pm 1\%$.

The test section was a 101.6×5.08 mm (9.67 mm hydraulic diameter) by 3.4 m long duct constructed of type 304 stainless steel. The liquid feed in the test section was made up of two porous sections of the side walls and the gas feed was made up of an axial length of piping attached to the bottom of the test section. The gas and liquid exited through a porous wall section near the top of the test section and through piping attached to the top of the test section. Three pairs of fused-silica windows, including one large pair, were installed in the test section for flow observation and for illumination of the droplets in the core region. The test section dimensions were selected to provide a small hydraulic diameter with a relatively large cross-section for ease of optical access and reduction of pressure drop, while addressing structural concerns regarding the fused-silica windows.

Pressure taps were located at nine locations between the liquid feed section and the lowest observation window pair along a vertical line displaced 25.4 mm from the center of the 101.6 mm wide wall. The tap locations were at positions 10.8, 28.6, 46.4, 64.0, 81.9, 99.7, 117.5, 135.3 and 153 cm above the liquid entry section. Eight pressure drop measurements were made with Rosemount Model 3051C differential pressure transmitters between the lowest pressure tap and each of the taps located above it (from 10.8 to 28.6 cm, 10.8 to 46.4 cm, etc.). Each of these measurements was considered accurate within $\pm1\%$. All differential pressures were digitized at three samples per second and digitally filtered to smooth out time-dependent fluctuations. The time series of the smoothed differential pressures were observed until they reached steady values, at which time each was recorded to a disk file along with the flow rates, miscellaneous temperatures and system gage pressures.

2.2. Drop size measurement technique

The droplet sizes were measured directly from video taken under annular flow conditions. The water film was removed through 7.62 cm tall porous wall sections as shown in Fig. 2 to help provide a clear image of the gas-droplet core. An Infinity Infinivar zoom microscope mounted to a Cohu model 4912-2100/000 monochrome CCD camera was used to view and videotape the droplets through the exit window, which was purged with nitrogen through small ports which are not shown in the diagram. A Kodak MAS strobe with a flash duration of 20 μs and average power of 400 W was used to illuminate the droplets from the side of the test section through a 3.81 cm tall window located 9.62 cm above the top of the porous wall section. The strobe was triggered externally at a frequency of 60 Hz by a pulse generator and the electronic shutter of the camera

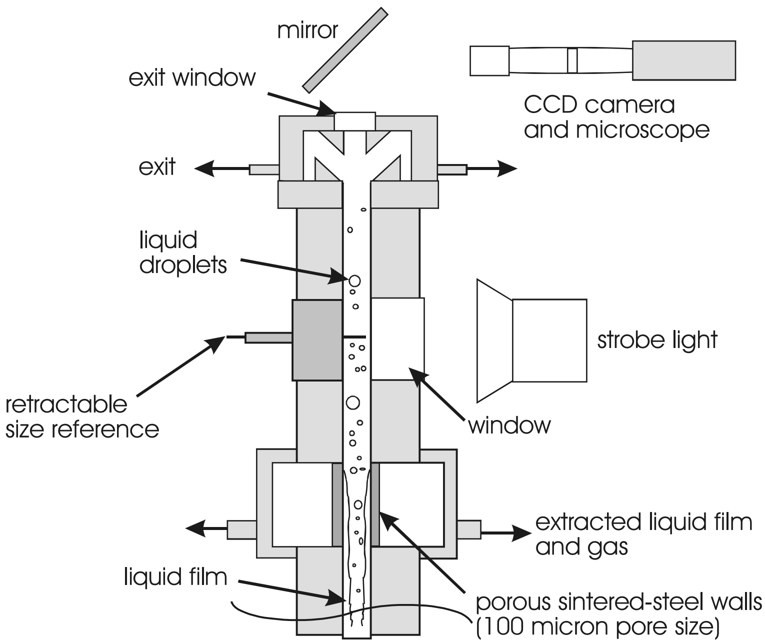

Fig. 2. Optical setup of viewing of droplets.

was kept continuously open, so that precise synchronization was not necessary. A retractable size reference was positioned within the test section and its image recorded at the beginning of any extended period of testing. The size reference was a 1.6 mm diameter steel rod with five lines scribed around its circumference at increments of 1 mm to form a graduated scale. Two minutes of video were recorded for each flow condition, producing a series of essentially still images. For conditions with clear droplet images, a number of frames were digitized with a Coreco Ultra II frame grabber card, all individual droplets identified manually and the drop sizes measured using a custom macro within Optimas (v. 6.0) image processing software.

The CCD camera, operated in interlaced field mode, produced a video image of 580 horizontal by 350 vertical lines. The camera captures 60 half-frames of video per second, where each half-frame alternates between odd and even horizontal lines. Each half-frame thus consists of 580 vertical by 175 horizontal lines. The horizontal lines determined the vertical resolution, while the vertical lines determine the horizontal resolution. The magnification achieved with the optical setup was evaluated by measuring the distance between lines on the size reference on an 20.3 cm high video monitor. On that monitor, the magnification was approximately $40\times$. With 175 lines, this resulted in a vertical resolution of 34.4 horizontal lines/mm or 0.029 mm/line (29 μm/line). The horizontal resolution is twice the vertical resolution, 68.8 vertical lines/mm or 0.015 mm/line. The resolution set a lower limit on the measurable drop size, such that drops smaller than 0.029 mm appear to be 0.029 mm in the vertical direction and drops smaller than 0.015 mm appear to be 0.015 mm in the horizontal direction. In practice, the smallest measurable drops were usually larger than 0.030 mm although a few smaller drops were measured and their size recorded. The size of the largest drops approached and exceeded 1 mm, depending on flow conditions. Since the drops at the lower end of the distribution carry little weight in the calculation of the Sauter mean diameter, it was more important to accurately measure the large drops.

Since the droplets were illuminated through a flat window, their images appeared similar at various positions within the test section, which would not have occurred with illumination through the curved surface of a tube. However, since the illumination was performed perpendicular to the viewing axis, the individual droplets did not always appear as complete circles. In most cases, the drops appeared as two opposing crescents or half-moons, separated by a dark band similar to the description given by Hay et al. (1996). In some cases, only one of the crescents appeared. For two crescents, the maximum distance between the outer edges of each crescent was measured and used to estimate the drop size with a calibration established using a recorded image of the size reference. For one crescent, the maximum top-to-bottom distance of the crescent was measured and used to estimate the drop size. The camera was oriented to achieve the highest resolution for the two-crescent case, so the opposing crescents both pointed vertically and the measured distance was in the horizontal direction. The best case single-drop accuracy is the resolution of the video camera and optics, ± 15 μm for two-crescent measurements and ± 30 μm for single-crescent measurements. Provided that enough measurements are taken and the measurement error is random, the accuracy in the higher-order means such as the Sauter mean become dependent more on the sample size than on the accuracy of the individual drop sizes as discussed below.

Large sample sizes are needed for accuracy in the higher-order means. As the order of the mean increases, the number of required samples for a certain accuracy also increases. Bowen and Davies estimated the accuracies for the Sauter mean diameter within 95% confidence limits based on the sample size (Azzopardi, 1997). In order to achieve accuracies better than ±5%, more than 5000 individual droplets are needed. For the less strict requirements of ±17% and ±10% accuracy, sample sizes of 500 and 1400, respectively, are required. With a few exceptions, most useful annular flow data sets in the literature are comprised of between 500 and 1400 samples. The sample sizes presented in this paper are between 800 and 2000.

The measurement volume for the drop size measurement is defined by the 101.6 × 5.08 mm cross-section of the test section and the depth-of-field of the microscope lens, which had a nominal value of approximately 10 mm. When the measurement volume is smaller than the droplets being measured, there is a measurement bias towards the larger droplet sizes. Since the measurement volume in this case is several times larger in each dimension than the largest droplets, there should be no significant bias from this effect.

2.3. Definitions

Two types of cumulative distribution functions are used to describe the statistics of dispersed drops. The cumulative size distribution function, F_d, describes the fraction of droplets below a certain size. The cumulative volume distribution function, F_v, describes the fraction of the total dispersed liquid volume present in droplets below a certain size. A probability density function (pdf) is associated with each of these cumulative distribution functions. The size pdf, $f_d(d)$, is defined as the probability that a droplet from the distribution will have a diameter of d. The volume pdf, $f_v(d)$, is calculated from the size pdf as

$$f_v(d) = \frac{d^3 f_d(d)}{\int_0^{d_{\max}} x^3 f_d(x)\,\mathrm{d}x} \tag{1}$$

from which the cumulative volume distribution function, F_v, is calculated as

$$F_v(d) = \int_0^d f_v(x)\,\mathrm{d}x. \tag{2}$$

For specific applications, the drop size distribution can be represented by a single weighted mean size. Mugele and Evans (1951) provide a general definition of the various mean drop sizes and their particular applications. The general definition is

$$d_{pq} = \left[\frac{\int_0^{d_{\max}} x^p f_d(x)\,\mathrm{d}x}{\int_0^{d_{\max}} x^q f_d(x)\,\mathrm{d}x}\right]^{1/(p-q)}, \tag{3}$$

where p and q are non-negative integers. For a sufficiently large sample size, the mean drop sizes can be calculated from the collection of drops directly using

$$d_{pq} = \left[\frac{\sum_{j=1}^{N} d_j^p}{\sum_{j=1}^{N} d_j^q}\right]^{1/(p-q)}. \tag{4}$$

The arithmetic number mean, d_{10}, is useful mainly for rough comparisons, while the Sauter mean, d_{32} or SMD, is the mean drop size most commonly reported and used in momentum, heat and mass transfer applications. The Sauter mean is the drop size that has the same volume-to-surface area ratio as the entire drop size distribution. Other mean sizes used in limited application include the surface mean, d_{20}, and the volume mean, d_{30}. Another statistic commonly reported and used mainly to characterize distributions is the volume median, d_{vm}, which represents the 50th percentage point in the cumulative volume distribution, $F_v(d_{vm}) = 0.5$. The general rule,

$$d_{10} < d_{20} < d_{30} < d_{32} \tag{5}$$

can be proven mathematically, and the volume median is usually larger than the Sauter mean.

3. Results and analysis

3.1. Test conditions

The flow loop was operated at two absolute pressures, 3.4 and 17 atm, established at the separator, and at a temperature of 38 °C established at the test section inlet. The water flow rate was varied between 0.0157 and 0.126 kg/s for corresponding superficial liquid velocities, U_{LS}, of 0.03 and 0.12 m/s. At the 3.4 atm separator pressure, the superficial gas velocity, U_{GS}, was varied between approximately 7 and 23 m/s at the measurement location. At the higher pressure of 17 atm, the superficial gas velocity was varied between approximately 5 and 12 m/s. Measurements were performed only for conditions that resulted in clear images of the droplets. This condition was dependent on the ability of the purging system to keep the upper window clear of droplets, which was directly dependent on a combination of liquid and gas flow rates. As the water flow rate was increased, the maximum gas flow rate at which the window remained clear decreased.

3.2. Distributions and mean sizes

The size pdf for each run was estimated from the collection of drop sizes by constructing a normalized size histogram. The range of the measured drop sizes was divided into a number of size classes of equal width, W, and the number of droplets within each size class was counted. The count from each size class was then divided by the total number of drops multiplied by the class width, resulting in an estimate of the droplet size pdf. Symbolically, this calculation is represented by

$$f_d(d_j) = \frac{N_j}{NW}, \tag{6}$$

where N_j is the number of drops with sizes in the range $d_j \pm W/2$ and N is the total number of drops. The volume pdf and the cumulative distributions were then calculated with discrete versions of the continuous function definitions. The accuracy in the pdf for a particular size class is dependent on the number of drops within that size class as illustrated below.

Neglecting bias errors, the standard error for a point in the discrete size pdf is taken from Bendat and Piersol (1986) as

$$\mathrm{SE}[\widehat{f}_d(d_j)] \approx \left[\frac{f_d(d_j)}{NW}\right]^{1/2} = \frac{f_d(d_j)}{\sqrt{N_j}}. \tag{7}$$

Two standard errors in the positive and negative direction from the estimated pdf represent the 95% confidence interval. This equation clearly shows the importance of the number of samples within an individual size class. Taking the discrete definition of the volume pdf, the corresponding standard error can be approximated as

$$\mathrm{SE}[\widehat{f}_v(d_j)] = \mathrm{SE}\left[\frac{d_j^3 f_d(d_j)}{W\sum_{k=1}^{N} d_k^3 f_d(d_k)}\right] = \frac{f_v(d_j)}{\sqrt{N_j}}. \tag{8}$$

For both the size and volume pdfs, the largest relative or percentage errors occur at larger sizes, where increasing size classes include progressively fewer droplets. In the size pdf, the value of f_d decreases with increasing size class so that the absolute uncertainty at the larger size classes is small for a sufficient sample size. However, since the volume pdf is weighted by the cube of droplet size, the absolute uncertainties with the same sample size can be very large for the largest size classes, which may also correspond to the largest values of f_v. A sample plot of size and volume pdfs for the same conditions is provided in Fig. 3, in which the number of droplets sampled was greater than 2000. The size class width used for the calculation of the size pdf in this diagram was 20 μm, which effectively resolves the distribution at the smallest sizes. However, due to the larger uncertainty associated with the volume pdf, a size class width of 200 μm was necessary to produce the volume pdf shown in Fig. 3, which still shows significant scatter. This shows that the sample size requirement for an accurate volume pdf estimate is much stricter than the requirement for an accurate Sauter mean diameter. For this reason, volume probability functions derived from limited sample size data sets should be used with caution.

The cumulative distribution function of droplet size is calculated from the discrete pdf as

$$F_d(d_j) = W\sum_{k=1}^{j} f_d(d_k), \tag{9}$$

with a similar equation for the cumulative distribution function for volume. The standard error for a cumulative distribution function is estimated using a propagation of uncertainty analysis as

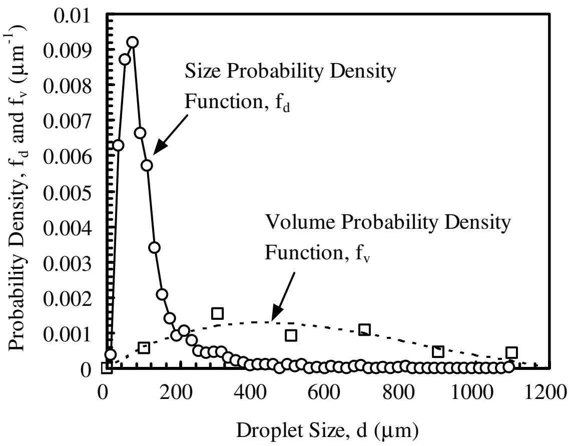

Fig. 3. Size and volume pdfs (liquid superficial velocity = 0.03 m/s; gas superficial velocity = 18.8 m/s; pressure = 3.6 atm).

$$\mathrm{SE}[F_d(d_j)] = \mathrm{SE}\left[W\sum_{k=1}^{j} f_d(d_k)\right] = W\left[\sum_{k=1}^{j}(\mathrm{SE}[f_d(d_k)])^2\right]^{1/2}, \tag{10}$$

which, after substituting the intermediate definition of the standard error for f_d, simplifies to

$$\mathrm{SE}[F_d(d_j)] = \sqrt{\frac{F_d(d_j)}{N}}. \tag{11}$$

The maximum standard error occurs at $F_d = 1$ and depends on the total number of drops in the distribution. For a total of 1000 drops, the 95% confidence interval for F_d or $F_v = 1.0$ is 1.0 ± 0.063, while for 2000 drops, it is 1.0 ± 0.045. The cumulative size and volume distributions for the same data set in Fig. 3 are shown in Fig. 4. There is less random variation in the cumulative volume distribution than in the pdfs due mainly to the different form of the standard error.

Due to the variable and sometimes significant uncertainty in the pdf estimates, the mean drop sizes were calculated directly from the collection of individual drop sizes and not from the computed pdf's. To determine whether the sample size was adequate for the SMD computation, the SMD was calculated as a running average from the first to the last drops measured during each run in a manner suggested by Lopes and Dukler (1985). A sample plot of this calculation is shown in Fig. 5 along with the 95% confidence limits. The calculated SMDs appear to have reached asymptotic values, providing some limited validation that the sample sizes are adequate, while the fluctuations in the running average remain for the most part within the confidence limits.

Table 1 contains the flow conditions, mean pressure gradient and calculated mean drop sizes for each run. The behavior of the number mean size, d_{10}, with increasing gas velocity is not as systematic as the behavior of the higher-order means, due to the smallest drops that were missed in the analysis. Those smallest drops can be nearly neglected for an accurate estimate of the SMD, however, due to the heavy weighting of the largest drop sizes in the calculation.

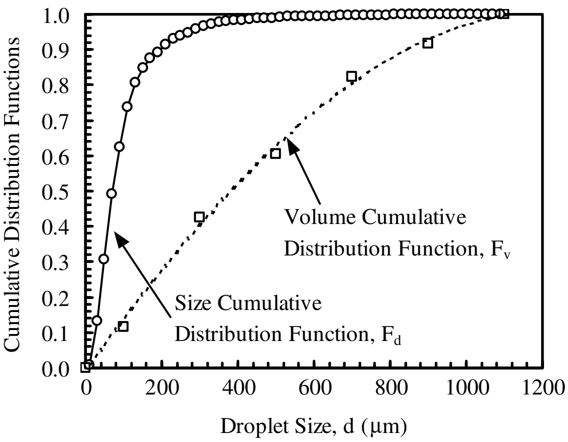

Fig. 4. Size and volume cumulative distribution functions (liquid superficial velocity = 0.03 m/s; gas superficial velocity = 18.8 m/s; pressure = 3.6 atm).

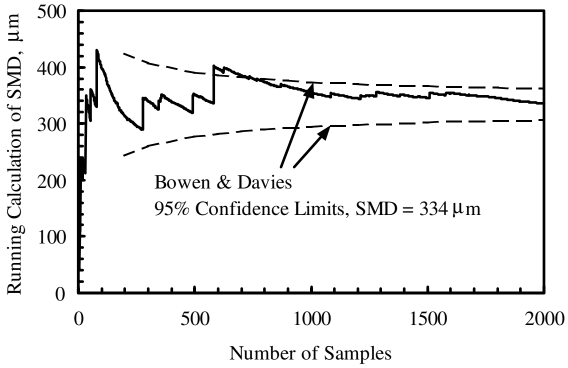

Fig. 5. Running calculation of Sauter mean diameter (liquid superficial velocity = 0.03 m/s; gas superficial velocity = 18.8 m/s; pressure = 3.6 atm).

Table 1
Mean drop sizes

U_{LS} (m/s)	U_{GS} (m/s)	P (atm)	T (°C)	$-dp/dx$ (Pa/m)	d_{10} (μm)	d_{20} (μm)	d_{30} (μm)	d_{32} (μm)	d_{vm} (μm)	d_{max} (μm)	Sample size
0.029	6.9	3.4	37	2300	268	361	457	728	858	1778	899
0.029	9.6	3.5	36	1510	236	313	390	601	706	1308	963
0.030	11.3	3.5	37	1653	134	195	280	572	723	1578	937
0.029	13.9	3.5	36	1797	109	149	205	386	534	1073	1420
0.030	16.1	3.5	37	2516	121	165	214	358	423	860	1003
0.030	18.8	3.6	37	2947	107	141	188	334	450	1083	2034
0.031	20.7	3.6	38	3558	111	143	183	298	365	754	1317
0.030	22.5	3.7	37	3882	123	157	195	300	351	888	1138
0.061	6.8	3.4	38	3127	288	376	466	714	888	1604	1191
0.061	9.3	3.5	38	2732	225	298	372	581	682	1495	1442
0.060	11.4	3.5	38	2840	231	295	357	522	595	1243	1284
0.062	13.7	3.6	38	3163	160	215	275	449	579	1048	1607
0.060	15.9	3.5	38	3522	155	204	255	400	464	967	1039
0.060	18.6	3.6	38	4098	185	225	266	370	415	871	1235
0.122	6.9	3.4	38	4026	280	365	462	739	871	2651	1257
0.121	9.3	3.5	38	4205	275	348	431	658	746	2198	1761
0.123	11.6	3.5	38	4565	255	324	392	575	651	1721	1132
0.245	6.8	3.5	38	5427	319	412	515	806	972	2175	1084
0.246	9.1	3.6	39	5859	251	321	391	581	682	1674	1614
0.030	4.6	17.3	38	1977	202	340	482	967	1120	2190	1018
0.030	6.9	17.3	37	2300	138	204	289	575	811	1347	1130
0.031	9.2	17.4	37	3379	165	229	296	492	568	1213	1047
0.030	11.3	17.6	37	4385	141	202	260	432	491	967	1071
0.061	4.5	17.4	39	2804	307	436	563	937	1113	2502	796
0.060	6.8	17.3	38	3271	236	339	456	823	1140	2104	1092
0.062	9.1	17.4	38	4277	254	331	411	635	738	1537	1094
0.063	11.4	17.6	38	6146	199	262	320	473	507	1196	1141
0.122	4.6	17.4	38	4313	380	512	653	1060	1242	3078	1074
0.122	6.9	17.4	38	4996	325	428	538	851	996	2657	1115
0.123	9.1	17.4	38	5859	333	417	500	718	801	2169	1207

3.3. Comparison with drop size correlations

Correlations for various mean droplet sizes in annular flow have been developed by a number of researchers using local flow conditions and fluid properties. Tatterson et al. (1977) developed a correlation using their own data combined with that of Wicks and Dukler (1966) and Cousins and Hewitt (1968). The Tatterson et al. correlation relates the volume median diameter to flow variables, physical properties, and the hydraulic diameter, D, as

$$\frac{d_{vm}}{D} = 0.016\left[\frac{\rho_G U_G^2 f_G D}{2\sigma}\right]^{-1/2}, \tag{12}$$

where ρ_G is the gas density, U_G is the gas velocity, f_G is a single-phase gas friction factor and σ is the surface tension. This correlation can be rearranged by using the gas Reynolds number, $Re_G = \rho_G U_G D/\mu_G$, a single-phase friction factor correlation, $f_G = 0.046/Re_G^{0.2}$, and a gas Weber number, $We_G = \rho_G U_G^2 D/\sigma$, into the form,

$$\frac{d_{vm}}{D} = 0.106 We_G^{-1/2} Re_G^{1/10}. \tag{13}$$

A comparison of the current data with this correlation is shown in Fig. 6. Included in this comparison are the data sets of Fore and Dukler, Cousins and Hewitt and Wicks (1967), which are summarized in Table 2. While the correlation line passes through the Wicks and Cousins and Hewitt data, from which it was developed, it underpredicts the current data obtained at significantly higher pressures.

Kataoka et al. (1983) used the Ishii and Grolmes (1975) mechanism for the inception of entrainment to build a correlation mainly from the data of Cousins and Hewitt and Wicks and Dukler. This correlation relates a Weber number based on the volume median diameter to the gas and liquid Reynolds numbers, fluid densities and fluid viscosities as

$$\frac{\rho_G U_G^2 d_{vm}}{\sigma} = We_{vm} = 0.028 Re_L^{-1/6} Re_G^{2/3}\left(\frac{\rho_G}{\rho_L}\right)^{-1/3}\left(\frac{\mu_G}{\mu_L}\right)^{2/3}. \tag{14}$$

This correlation can also be rearranged with the use of the gas Weber number as

$$\frac{d_{vm}}{D} = 0.028 We_G^{-1} Re_L^{-1/6} Re_G^{2/3}\left(\frac{\rho_G}{\rho_L}\right)^{-1/3}\left(\frac{\mu_G}{\mu_L}\right)^{2/3}. \tag{15}$$

The current set of data, combined with the data summarized in Table 2, is compared with this correlation in Fig. 7. Like the Tatterson et al. correlation, this correlation passes through the middle of the data from which it was developed. Similarly, the current data points at a pressure of 3.4 atm fall around the correlation line with significant scatter but with the correct trend. However, the data obtained at a pressure of 17 atm, as well as the Fore and Dukler data obtained at a higher liquid viscosity, fall significantly above the correlation line. This difference indicates that the effects of gas density and liquid viscosity are not properly accounted for by the Kataoka et al. correlation. This result is not surprising, since all of the data used to build the Kataoka et al. correlation were obtained using air and water at pressures between 1 and 2 atm.

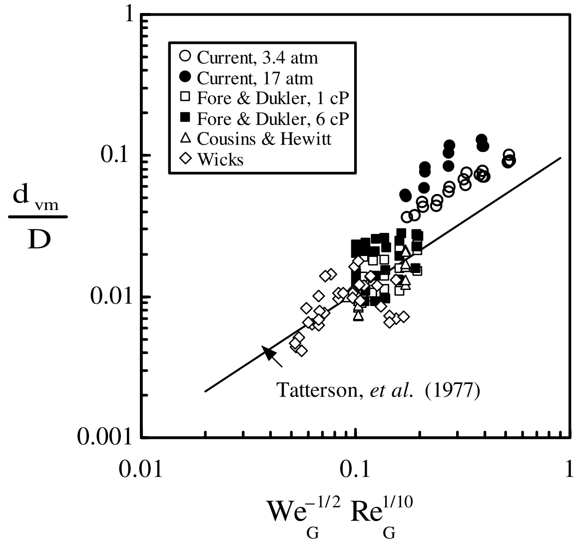

Fig. 6. Comparison of volume median droplet sizes with Tatterson et al. (1977) correlation.

Table 2
Data sets used for comparison

Data set	Geometry	Fluid system	ρ_L/ρ_G	μ_L/μ_G
Current, 3.4 atm	101.6 × 5.08 mm duct	Nitrogen–water	250	37
Current, 17 atm	101.6 × 5.08 mm duct	Nitrogen–water	50	37
Fore and Dukler (1995) 1 cP	50.8 mm tube	Air–water	800	56
Fore and Dukler (1995) 6 cP	50.8 mm tube	Air–water/50% glycerine	860	333
Cousins and Hewitt (1968)	9.53 mm tube	Air–water	410	56
Wicks (1967)	152.4 × 19.05 mm duct	Air–water	848	56

Kocamustafaogullari et al. (1994) used Sevik and Park's (1973) theory for turbulent drop breakup, as applied by Lopes and Dukler (1985), to develop a correlation for the maximum droplet size in annular flow. They used the maximum drop sizes reported by Lopes and Dukler to obtain

$$\frac{d_{max}}{D} = 2.609 C_W^{-4/15} We_G^{-3/5} (Re_G^4/Re_L)^{1/15} [(\rho_G/\rho_L)(\mu_G/\mu_L)]^{4/15}, \tag{16}$$

where

$$C_W = 0.028 N\mu^{-4/5} \quad \text{for } N\mu \leqslant 1/15, \tag{17}$$

and

$$C_W = 0.25 \quad \text{for } N\mu > 1/15. \tag{18}$$

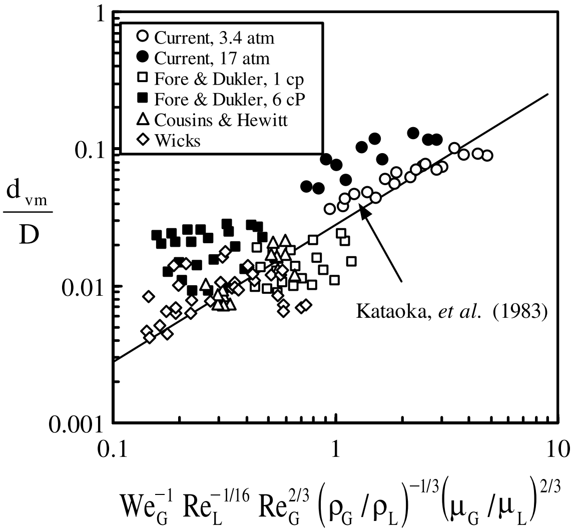

Fig. 7. Comparison of volume median droplet sizes with Kataoka et al. (1983) correlation.

The viscosity number, $N\mu$, is defined by

$$N\mu = \frac{\mu_L}{\left[\rho_L\sigma(\sigma/g\Delta\rho)^{1/2}\right]^{1/2}}. \tag{19}$$

A comparison with this correlation is shown in Fig. 8. The correlation groups the current drop sizes obtained at the two pressures of 3.4 and 17 atm, with some scatter, and passes through the middle of the Fore and Dukler and Cousins and Hewitt data. All of the Wicks data lie above the line. Kocamustafaogullari et al. assumed the droplet sizes followed the upper-limit log-normal distribution used by Wicks and Dukler (1966) among others, in order to develop a correlation for the Sauter mean diameter,

$$\frac{d_{32}}{D} = 0.65C_W^{-4/15}We_G^{-3/5}(Re_G^4/Re_L)^{1/15}[(\rho_G/\rho_L)(\mu_G/\mu_L)]^{4/15}. \tag{20}$$

A comparison with this correlation is shown in Fig. 9. The Sauter mean diameters obtained at pressures of 3.4 and 17 atm are underpredicted, although the form of the correlation does effectively group them together. Since the maximum drop sizes are represented well by the Kocamustafaogullari et al. correlation in equation (19), the difference in the Sauter mean diameter is probably due to the assumption that the drop sizes follow a fixed type of distribution. Otherwise, the coefficient in the correlation (20) can be changed from 0.65 to 1.3 in order to pass through the new data and some of the Fore and Dukler data as shown in Fig. 9. However, significant scatter and disagreement with the Wicks and Cousins and Hewitt data sets remain even after this adjustment.

From the above comparisons, mean drop sizes from the two simple geometries of circular tubes, represented by the Cousins and Hewitt and Fore and Dukler data, and wide-wall ducts, represented by the Wicks and current data, follow very similar trends when normalized by the

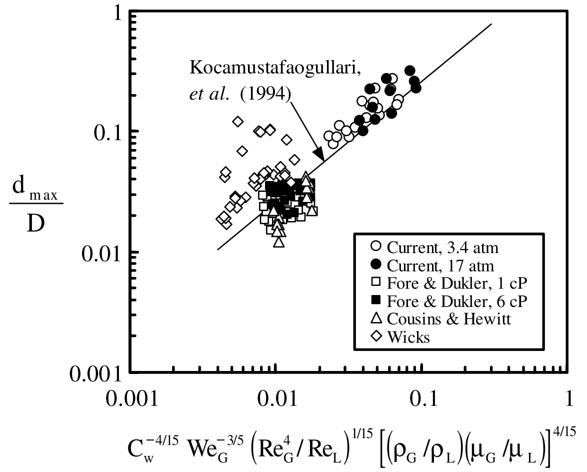

Fig. 8. Comparison of maximum droplet sizes with Kocamustafaogullari et al. (1994) correlation.

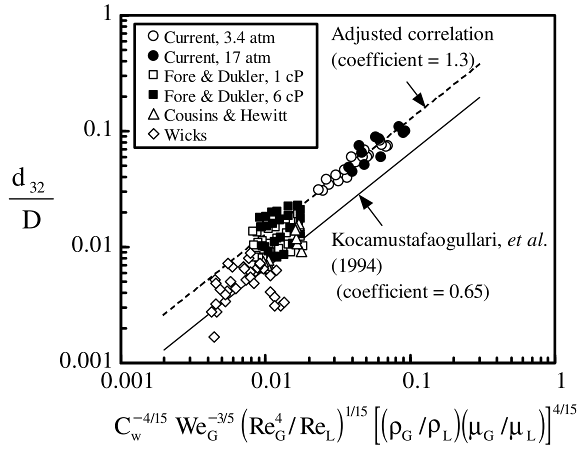

Fig. 9. Comparison of Sauter mean diameters with Kocamustafaogullari et al. (1994) correlation.

hydraulic diameter. Any effect of geometry is buried within the scatter of the data around the correlations. Since the mechanisms governing droplet size in annular flow, including any geometry or upstream history effects, are likely more complex than represented by the simplified correlations of Figs. 6–9, some level of scatter should be fully expected.

4. Summary

Drop size distributions have been measured for nitrogen–water annular flow in a 9.67 mm hydraulic diameter duct, at system pressures of 3.4 and 17 atm and at a temperature of 38 °C.

These new measurements extend the range of conditions represented by existing annular flow droplet size data in the open literature, primarily through an increase in system pressure and gas density. Since most existing correlations were developed from drop size data obtained at lower pressures and gas densities, it should be expected that the higher-pressure measurements presented in this paper would not necessarily follow those correlations. Hence, the correlation of Tatterson et al. (1977) does not predict the current measurements very well, while the correlation of Kataoka et al. (1983) only predicts the drop sizes measured at the lower pressure of 3.4 atm. The maximum drop size correlation of Kocamustafaogullari et al. (1994) does agree in trend and magnitude with the new measurements. A correlation for the Sauter mean diameter derived from this maximum drop size correlation agrees with the new measurements, provided the leading coefficient in the correlation is modified from the original.

References

Ambrosini, W., Andreussi, P., Azzopardi, B.J., 1991. A physically based correlation for drop size in annular flow. Int. J. Multiphase Flow 17, 497–507.

Azzopardi, B.J., 1997. Drops in annular two-phase flow. Int. J. Multiphase Flow 23, 1–53.

Azzopardi, B.J., Teixeira, J.C.F., 1994. Detailed measurements of vertical annular two-phase flow—Part I: Drop velocities and sizes. Trans. ASME: J. Fluids Eng. 116, 792–795.

Azzopardi, B.J., Freeman, G., King, D.J., 1980. Drop sizes and deposition in annular two phase flow. UKAEA Report, AERE-R9634.

Azzopardi, B.J., Piearcey, A., Jepson, D.M., 1991. Drop size measurements for annular two-phase flow in a 20 mm diameter vertical tube. Exp. Fluids 11, 191–197.

Bendat, J.S., Piersol, A.G., 1986. Random Data: Analysis and Measurement Procedures, second ed. (Revised and Expanded) John Wiley & Sons, New York.

Cousins, L.B., Hewitt, G.F., 1968. Liquid phase mass transfer in annular two-phase flow: droplet deposition and liquid entrainment. UKAEA Report, AERE-R5657.

Fore, L.B., Dukler, A.E., 1995. The distribution of drop size and velocity in gas–liquid annular flow. Int. J. Multiphase Flow 21, 137–149.

Hay, K.J., Liu, Z.-C., Hanratty, T.J., 1996. Relation of deposition to drop size when the rate law is nonlinear. Int. J. Multiphase Flow 22, 829–848.

Ishii, M., Grolmes, M.A., 1975. Inception criteria for droplet entrainment in two-phase concurrent film flow. AIChE J. 21, 308–318.

Kataoka, I., Ishii, M., Mishima, K., 1983. Generation and size distribution of droplet in annular two-phase flow. Trans. ASME: J. Fluids Eng. 105, 230–238.

Kocamustafaogullari, G., Smits, S.R., Razi, J., 1994. Maximum and mean droplet sizes in annular two-phase flow. Int. J. Heat Mass Transfer 37, 955–965.

Lopes, J.C.B., Dukler, A.E., 1985. Droplet sizes, dynamics and deposition in vertical annular flow. NUREG/CR4424; Also Lopes, J.C.B., 1984. Ph.D. dissertation, University of Houston.

Lopes, J.C.B., Dukler, A.E., 1987. Droplet dynamics in vertical gas–liquid annular flow. AIChE J. 33, 1013–1023.

Mugele, R.A., Evans, H.D., 1951. Droplet size distribution in sprays. Ind. Eng. Chem. 43, 1317–1325.

Semiat, R., Dukler, A.E., 1981. Simultaneous measurement of size and velocity of bubbles or drops: a new optical technique. AIChE J. 27, 148–159.

Sevik, M., Park, S.H., 1973. The splitting of drops and bubbles by turbulent fluid flow. Trans ASME: J. Fluids Eng. 95, 53–59.

Tatterson, D.F., Dallman, J.C., Hanratty, T.J., 1977. Drop sizes in annular gas–liquid flows. AIChE J. 23, 68–76.

Trabold, T.A., Kumar, R., Vassallo, P.F., 1999. Experimental study of dispersed droplets in high-pressure annular flows. J. Heat Transfer 121, 924–933.

Wicks, M., 1967. Liquid film structure and drop size distribution in two-phase flow. Ph.D. dissertation, University of Houston.

Wicks, M., Dukler, A.E., 1966. In situ measurements of drop size distribution in two-phase flow: a new method for electrically conducting liquids. In: Proc. 3rd Int. Heat Transfer Conf., vol. 5, pp. 39–48.